PCCP

PAPER

Cite this: *Phys. Chem. Chem. Phys.*, 2017, **19**, 24626

Dissociative adsorption dynamics of nitrogen on a Fe(111) surface

M. A. Nosir, *[ab] L. Martin-Gondre,[c] G. A. Bocan[d] and R. Díez Muiño[ab]

Received 1st June 2017,
Accepted 14th August 2017

DOI: 10.1039/c7cp03701e

rsc.li/pccp

We study the dissociative adsorption dynamics of N_2 on clean bcc Fe(111) surfaces. We base our theoretical analysis on a multidimensional potential energy surface built from density functional theory. The dissociative sticking probability is computed by means of quasi-classical trajectory calculations. For normal incidence and impact energies of the order of a few eV, our theoretical results agree well with existing experimental values. For these energies, the dynamics of the dissociated molecules shows that dissociation is a direct process that follows narrow paths in the multidimensional space. For lower energies of the beam, this direct process is not enough to explain the measured values. A better agreement with the experiment is obtained if we increase the surface temperature to promote the transfer to dissociation of molecules previously trapped. Most of the molecules dissociate very close to the Fe(111) third layer atoms and with an orientation parallel to the surface. A comparison between the dissociation of N_2 on Fe(111) and Fe(110) highlights the role of the different energy barriers in both surfaces.

1. Introduction

Ammonia synthesis is one of the most important catalytic reactions in the chemical industry.[1] The production of approximately 160 million tons of ammonia per year, a production process that accounts for 1–2% of the world's annual primary energy consumption,[2,3] explains why ammonia synthesis is one of the most investigated catalyzed reactions in surface chemistry. Inside the reactor, the interaction of H_2 and N_2 is usually catalyzed by iron based compounds, taking advantage of the low price and the relatively high reactivity of iron. The rate-determining step in ammonia synthesis on iron has been identified to be the dissociative adsorption of N_2.[4–10] Therefore, the study of the microscopic reaction steps in the N_2 dissociation on Fe surfaces is a topic of much interest.

In general, in the surface science approach, surface reactivity can be highly dependent on the geometry and electronic structure of the surface.[11,12] The reaction kinetics, for the same local electronic properties of the surface atoms, can be modified by the difference in bonding geometry.[13] Therefore, the chemical reactivity can be effectively enhanced or hindered depending on the particular arrangements of surface atoms. Tungsten surfaces, for instance, represent a clear example of the variation of reactivity when switching between two different W faces. Molecular beam experiments show that, at relatively low surface temperature and thermal energies of the incident molecules, the sticking coefficient S_0 for N_2 on W(110)[14] is lower by two orders of magnitude than the one on W(100), for which the sticking coefficient is $S_0 \approx 1$.[15–18] Alducin *et al.*[19,20] explained such a difference in terms of dynamical effects occurring at distances relatively far from the surface.

In the particular case that we treat in this work, namely, the interaction of nitrogen molecules with iron surfaces, previous studies revealed the same effect and concluded that the dissociation of N_2 molecules is very much dependent on the Fe crystal orientation.[11] As a consequence of this, at low pressure, the chemical activity of the low-index bcc-iron faces for ammonia formation varies. The most open surface Fe(111) is the most reactive one whereas the chemical reactivity is decreased for Fe(100) and further more in the closed packed Fe(110).[21]

In early works by Ertl *et al.*[22,23] several experimental techniques were used to study the nitrogen adsorption on the low index bcc-iron faces Fe(111), Fe(100) and Fe(110). In particular, for N_2 on Fe(111), they identified two weakly chemisorbed states. A weakly bound γ-state perpendicular to the Fe(111) surface and a more strongly bound parallel α-state, for which the nitrogen atoms have a stronger interaction with the surface atoms. An additional atomic β-state was also observed. They also reported a very small initial sticking coefficient for N_2/Fe(111) ($S_0 \approx 10^{-7}$–10^{-6}). Grunze *et al.* confirmed these findings and suggested that the nitrogen dissociation proceeds *via* a precursor state.[24] All subsequent experimental observations[25–29] reached similar conclusions. Over time, other molecular adsorption states were reported as well: Grunze *et al.* found a rarely

[a] *Centro de Física de Materiales CFM/MPC (CSIC-UPV/EHU), Donostia-San Sebastián, Spain. E-mail: mohamed_ahmed@ehu.es*
[b] *Donostia International Physics Center (DIPC), Donostia-San Sebastián, Spain*
[c] *Institut UTINAM – Univ. Bourgogne Franche-Comté, Besançon, France*
[d] *CONICET and Centro Atómico Bariloche (CNEA), Argentina*

occupied adsorption δ-state,[29] and Freund and coworkers observed an additional molecular adsorption ε-state.[28]

In recent years, total energy calculations based on density functional theory (DFT) have been performed for modeling the interactions of nitrogen atoms and molecules and the three low-index iron faces.[30–35] Calculations for the nitrogen adsorption features on Fe(111)[30,36–39] show quantitative as well as qualitative agreement with the experimental observations. This sort of static DFT calculation provides valuable information about possible adsorption states and can be used to estimate both the entrance and dissociation barriers. However, a detailed description of gas/surface elementary reaction processes is required to go beyond static DFT information and include dynamics. Therefore, molecular dynamics simulations based on the calculation of potential energy surfaces were performed for different systems. Goikoetxea *et al.* presented the first full dynamical study of N_2 on the less reactive crystal face of iron, namely Fe(110).[32] They performed the calculation on a six-dimensional DFT-based potential energy surface (6D-PES). They reported the effect of surface temperature as well as the initial conditions of the N_2 beam on the sticking probability. Despite the higher reactivity of Fe(111), to the best of our knowledge, there have been no full dynamical studies on the dissociation dynamics of N_2 on the Fe(111) surface.

The scientific and technological interest behind the interaction of N_2 with the Fe(111) surface makes a good case for a detailed study of the dynamical processes. In a previous study,[40] we performed electronic structure calculations for the Fe(111) surface relaxations and the preferred atomic N adsorption sites on Fe(111). In addition, the 6D-PES of the system was constructed combining DFT total energy calculations with multidimensional interpolation techniques. On the 6D-PES, we investigated the nitrogen molecular adsorption dynamics on Fe(111).[41] In the current article, we complete our series of studies on N_2/Fe(111) and present the dissociative adsorption dynamics of N_2 on Fe(111). A comparison with available experimental data[42] is made. A discussion on the difference between the high chemical reactivity of Fe(111) and the lower reactivity of the Fe(110) surface[32] is also included.

The article is arranged as follows: Section 2 describes the computational details used to perform quasi-classical calculations. In Section 3, calculations of the initial sticking probability for normal and off-normal incidence of the molecular beam, as well as details of the dissociative adsorption dynamics, are presented. A comparison between the reaction characteristics of nitrogen on Fe(111) and Fe(110) is shown in Section 4. The conclusion and outlook are included in Section 5.

2. Methodology

The theoretical methodology is very similar to the one presented in the previous study of molecular (non-dissociative) adsorption dynamics of N_2 on Fe(111).[41] For this reason, we just summarize it here.

The interaction energy between the nitrogen molecule and the iron surface is evaluated by performing spin polarized DFT calculations[43,44] as implemented in the Vienna Ab-initio Simulation Package (VASP),[45–47] which uses a plane-wave basis set for the description of the electronic wave functions. The Generalized Gradient Approximation (GGA)[48] is used to calculate the exchange–correlation (XC) energy, with the Perdew–Wang (PW91)[49] energy functional. The ion–core interactions are represented by the Projector Augmented Wave (PAW)[46,47] pseudo-potential method. A 400 eV cut-off energy is used for the expansion of the plane-wave basis set.

A supercell periodic slab is employed to represent the Fe(111) surface. A 2 × 2 unit cell, as shown in Fig. 1a, is used to model the Fe(111) surface. DFT calculations were performed within the frozen surface approximation and using a slab consisting of 9-layers. The three-dimensional Brillouin-zone integrations are performed by sampling the k-points with 6 × 6 × 1 Monkhorst–Pack grids,[50] which provide an adequate balance between numerical accuracy and computational burden.

We reported in a previous work[40] a calculated bulk lattice constant of a = 2.855 Å and a bulk modulus of B_0 = 184 GPa, in good agreement with the experimental values of 2.867 Å[51] and 168 GPa,[52] respectively. For a slab consisting of 9 layers and a distance between slabs of 15 Å, the net interlayer spacing values for Fe(111) are $d_{12} \approx 0.74$ Å, $d_{23} \approx 0.64$ Å, and $d_{34} \approx 0.90$ Å, where d_{ij} is the distance between the i- and j-layers, and the

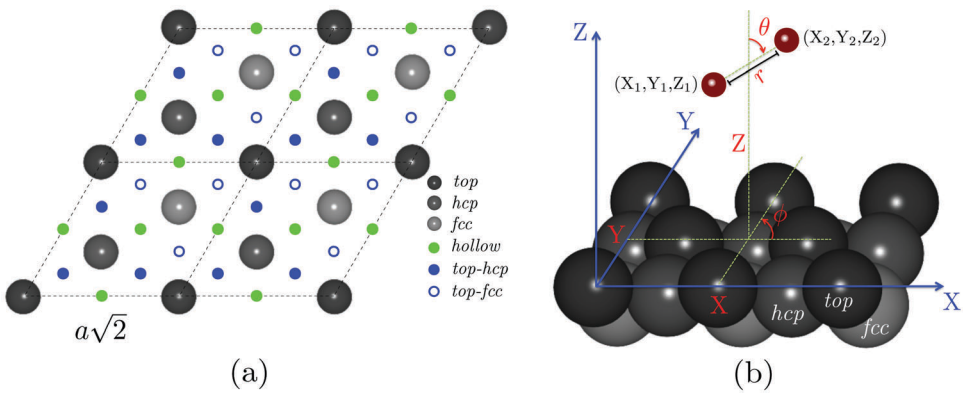

Fig. 1 (a) Top view of the 2 × 2 unit cell of Fe(111) and (b) representation of the coordinate system used to describe the N_2/Fe(111) interaction.

interlayer spacing of the bulk is $d_0 \approx 0.824$ Å. A detailed comparison of these theoretical values with available experimental information can be found in ref. 40.

The equilibrium internuclear distance for a nitrogen molecule in the gas phase is found to be $r_{eq} = 1.1125$ Å. The coordinate system of the N_2 molecule on Fe(111) is represented in Fig. 1b as follows: $(X,Y,Z)_{cm}$ define the position of the molecular center of mass, with (X,Y) the position on the surface plane and Z the perpendicular distance to the surface plane. The internuclear distance is defined as r, the polar angle θ represents the angle between the molecular axis and the surface normal, and the azimuthal angle ϕ defines the angle between the molecular axis projection on the XY plane and the X-axis. Over the high symmetry sites of the surface unit cell (top, hcp, fcc, hollow, top-hcp, and top-fcc), shown in Fig. 1a, a total number of 21420 DFT points are obtained systematically varying the molecule coordinates for different geometrical configurations.

Based on these DFT calculations, a global six-dimensional potential energy surface 6D-PES was built by a combination of interpolation techniques, a key ingredient of which is the corrugation reducing procedure (CRP). This method developed by Busnengo *et al.*[53,54] ensures an accurate interpolation even in highly corrugated 6D regions.[55] The CRP interpolation method consistently shows high accuracy over the six-degrees of freedom of the N_2/Fe(111) system.[41]

Quasi-classical trajectory (QCT) calculations are performed on the continuous 6D-PES in order to study the N_2 dissociative adsorption dynamics on the clean Fe(111) surface. We include the initial zero point energy (ZPE) of the molecule in the calculations and set it to ZPE = 142 meV. The path for all trajectories starts with the molecule at its internuclear equilibrium distance in the gas phase and with an initial distance from the surface of $Z_{cm} = 5.0$ Å, far enough for molecule–surface interactions to be negligible. A conventional Monte Carlo procedure is used for sampling the initial molecular coordinates (X,Y) and the molecular orientation (θ and ϕ). For surface motion, the generalized Langevin oscillator (GLO) model is applied to simulate surface temperature effects.[56–58] We closely follow the implementation of the GLO model proposed by Busnengo *et al.* in ref. 58, as done, for instance, in ref. 35 and 41. In brief, we describe the surface motion in terms of a three-dimensional harmonic oscillator. Energy dissipation is included through an additional 'ghost' oscillator that plays the role of a thermal bath.

In our calculations, we distinguish among three different events: (i) reflection, when the molecular center of mass reaches for a second time the initial starting distance of 5.0 Å, with positive velocity pointing towards the vacuum; (ii) dissociation, when the molecule bond length reaches the value of $r_{diss} = 2.1125$ Å with a positive radial velocity; and (iii) molecular trapping, when the molecule is neither reflected nor dissociated after 10 ps. The calculations are performed within a wide interval of initial kinetic energies for the molecule, ranging between 50 meV and 5.0 eV. For each value of the initial kinetic energy (E_i), a large number of trajectories (100 000) is used to obtain sufficiently good statistics, with a maximum trajectory integration time of 10 ps. The surface sampling area used for representing the initial impact (X,Y) positions on the surface is shown as the shaded area in Fig. 2.

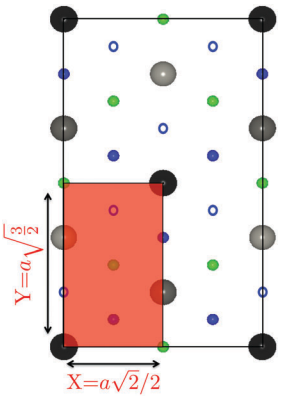

Fig. 2 Representation of the Fe(111) surface unit cell used in the quasi-classical trajectory calculations. The high symmetry sites of the surface unit cell (top, hcp, fcc, hollow, top-hcp, and top-fcc) are shown with the same color codes as in Fig. 1a. The shaded area illustrates the sampling area of initial (X,Y) positions of the incident N_2 molecule, where 'a = 2.855 Å' is the lattice parameter.

3. Results and discussion

Molecular trapping

Let us start this section by summarizing previous results on the atomic adsorption of N on Fe(111) and molecular (non-dissociative) adsorption of N_2 on Fe(111) that provide the necessary context for the analysis of dissociative chemisorption. In ref. 40, we reported that the only possible adsorption site for nitrogen atoms is the hollow site (green solid circles in Fig. 1a), called the β-state. Our calculations provide an adsorption energy for the β-state of $E_{ads} \approx -5.82$ eV. Other theoretical[30–33] and experimental[22,23,59] studies offer adsorption energy values that vary from −6.6 eV to −5.7 eV. From the static analysis presented in ref. 41, four molecular adsorption states were found, namely, γ, δ, α, and ε. Fig. 3 shows a schematic representation of the four possible molecular adsorption states as well as the atomic adsorption one.

A dynamical analysis based on quasi-classical trajectory (QCT) calculations, also performed in ref. 41, showed that the N_2 molecular adsorption probability is highly dependent on the initial molecule impact energy, being much higher (close to 1) for low initial energies of the incoming molecule. Most of the molecules in this low energy regime are adsorbed into the γ-state. The surface temperature also affects the adsorption probability. For relatively high surface temperature (520 K), a large number of molecules were recorded as dynamically trapped after reaching the calculation time of 10 ps. When increasing the impact energy, molecules are able to overcome existing energy barriers and can reach the other parallel adsorption states (α and ε). Previous studies on N_2/Fe(111) discussed the dissociation process *via* a precursor state.[24] The intermediate precursor state suggested was a molecule adsorbed parallel to the surface, with a geometry in which the two N atoms are strongly attracted to the surface.

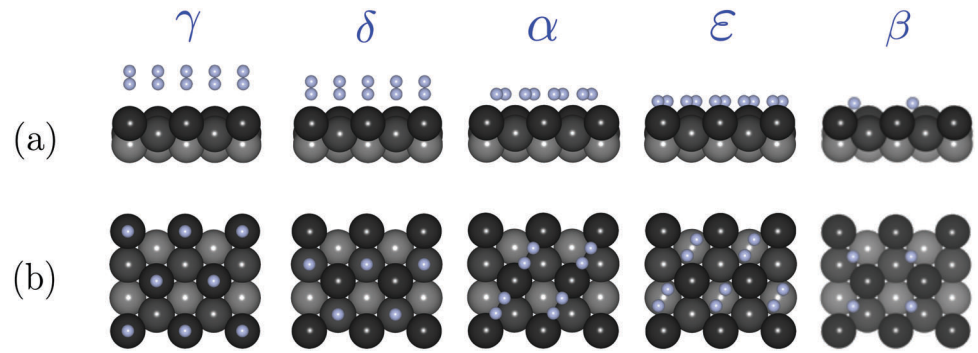

Fig. 3 (a) Side view and (b) top view of the five nitrogen adsorption states on a clean Fe(111) surface. From left to right, γ, δ, α, and ε are the molecular adsorption states and β is the atomic adsorption state.

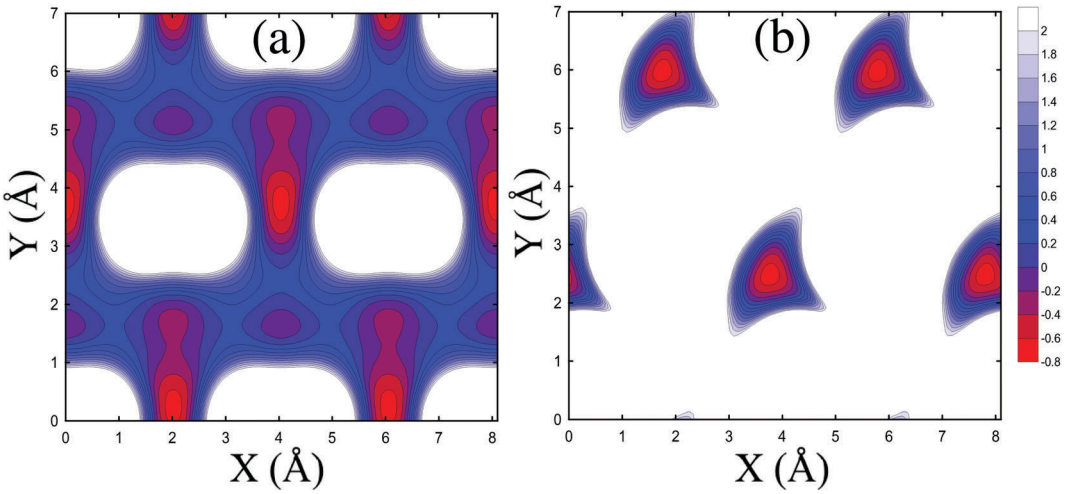

Fig. 4 Two dimensional (X_{cm},Y_{cm}) cuts of the interpolated 6D-PES for the α and ε adsorption states. (a) α-state with Z_{cm} = 1.2 Å, r = 1.213 Å, θ = 90° and ϕ = 0°. (b) ε-state with Z_{cm} = 0.6 Å, r = 1.313 Å, θ = 90° and ϕ = 60°. The energy scale to the right is given in eV, ranging from −0.8 eV (red) to 2.0 eV (blue). The white regions show potential energy values higher than 2.0 eV. The contour lines are separated by an interval of 0.2 eV.

The characteristics of the adsorption into the α and ε-states fulfill these conditions and could therefore be of importance for the molecular dissociation process. For this reason, we present in Fig. 4 the 2D contour plots of the interpolated 6D-PES for the α (Fig. 4a) and ε (Fig. 4b) states.

Dissociative dynamics of N_2 on Fe(111)

In the following we present our results for the quasi-classical trajectory calculations of N_2 dissociative adsorption dynamics on the clean Fe(111) surface. In Fig. 5, the initial sticking probability S_0 is shown as a function of the initial kinetic energy of the molecule, for a surface temperature of T_s = 520 K. Results are shown for normal (Θ_i = 0°) and off-normal incidence angles (Θ_i = 30°, 60°). In general, for the number of trajectories considered, no dissociation events were found below E_i = 800 meV. S_0 increases when the initial molecule impact energy is increased. In Fig. 5a, the sticking probability is plotted as a function of the total energy and it is observed that S_0 decreases as the initial impact angle deviates from the normal incidence. In Fig. 5b, the sticking probability is plotted as a function of the normal energy ($E_i \cos^2 \Theta_i$) and we verify that normal energy scaling does not apply in this case, suggesting that dissociation is not a direct process.

The dissociation of N_2 on Fe(111) has been experimentally studied using molecular beam techniques.[42] In ref. 42, Auger-electron spectroscopy (AES) was used to identify the adsorbed species and study the effect of the initial kinetic energy of the N_2 molecule on the initial sticking probability at the Fe(111) surface, with T_s = 520 K and for normal incidence. The measured initial sticking probabilities were determined from the initial slopes of coverage *versus* exposure curves in the AES spectra. Fig. 6 illustrates the variation of the initial sticking probability S_0 *versus* the initial impact energy for normal incidence. A comparison between our theoretical work and the experimental observation is shown. Theoretical results in Fig. 6 are shown for surface temperatures of 520 K and 2000 K.

Let us first focus on the N_2 dissociative adsorption curve for T_s = 520 K. Within the statistical error, the sticking probability is zero for kinetic energies below 0.80 eV. In the intermediate energy range, the sticking probability monotonically increases with the initial kinetic energy. For E_i > 4 eV, S_0 matches the experimental measurements, while for lower energies, the calculated

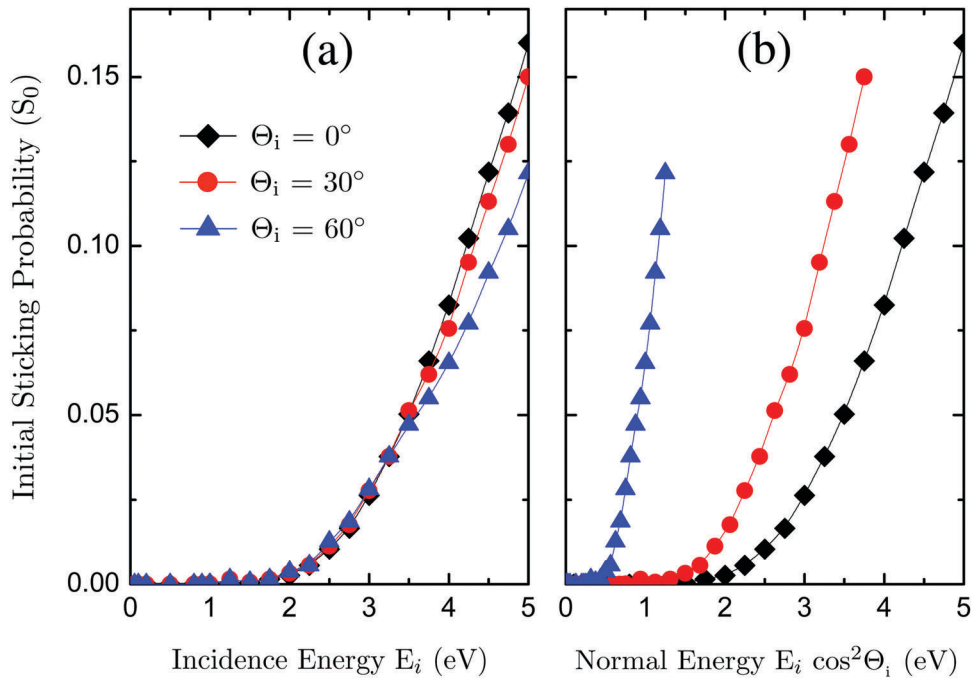

Fig. 5 Dependence of the initial sticking probability S_0 on the initial incidence kinetic energy E_i for different incidence angles Θ_i: (a) as a function of the initial impact energy and (b) as a function of the normal energy.

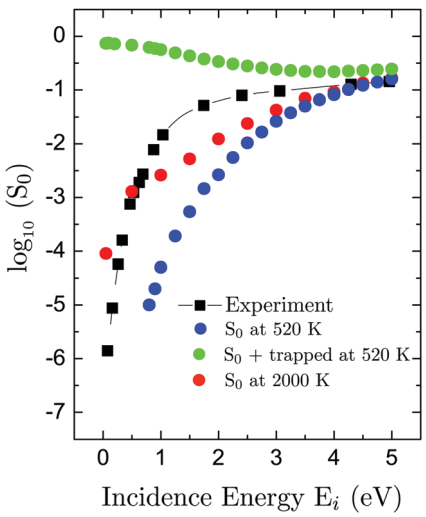

Fig. 6 Initial sticking probability S_0 as a function of the initial impact energy E_i for normal incidence. Black squares are experimental data.[42] Blue, green, and red circles are our theoretical results of S_0, the sum of S_0 and the trapping probability for a surface temperature of T_s = 520 K, and S_0 for T_s = 2000 K, respectively.

sticking probabilities in Fig. 6 are slightly lower than the experimental ones. One possible reason for this difference is that the upper limit of our calculation time (10 ps) could be insufficient to simulate the full dynamics of the process and, hence, to obtain the probability of the final reactive and non-reactive channels. After 10 ps, some of the molecules remain dynamically trapped in the vicinity of α and ε adsorption wells (see Fig. 11 in ref. 41). The trapped molecules are localized in these regions until they gain enough energy to become either dissociated or reflected to the gas phase. Such a process may require much longer simulation times. To give an idea of the relevance of this process, we also plot in Fig. 6 the sum of the computed dissociative probability S_0 plus the probability of finding N_2-trapped molecules at the surface of T_s = 520 K after 10 ps (green solid circles).

We have tried to estimate the final fate of these dynamically trapped molecules by increasing the surface temperature. An increase in surface temperature results in a large decrease in dynamically trapped molecules because energy exchange with the surface phonons is favored and the lifetime of the dynamically trapped state is shortened.[58] Therefore, we have performed QCT calculations at a surface temperature of T_s = 2000 K. Such an unrealistic value of the surface temperature implies that no trapped molecules remain within our calculation time limit of 10 ps. This result confirms the assumption in our previous study[41] that increasing T_s leads to a decrease of the trapped molecules through either reflection or dissociation. As shown in Fig. 6, the S_0 values of T_s = 2000 K results are closer to the experimental data in the intermediate kinetic energy regime. The reason is that, for a higher surface temperature, some of the trajectories that were dynamically trapped are now eventually dissociated. Furthermore, the majority of the primary-trapped molecules end up reflected with increasing T_s. The translation of this conclusion to the dynamics at T_s = 520 K has to be made with some caution, however. An increase in the surface temperature is not only a way of shortening the time for the dissociation process but it can also modify the dynamics.

In our calculations we have verified that most of the dissociation events proceed *via* a direct mechanism in the high energy range.

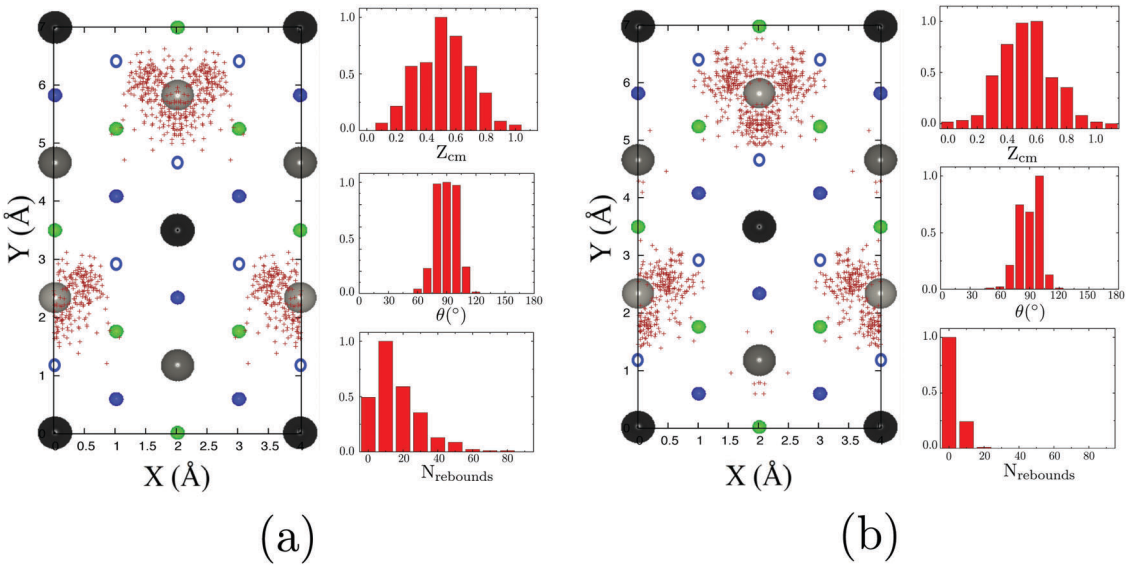

Fig. 7 Left panel: Position (*X*,*Y*) of the center of mass of the dissociated molecules at the time of dissociation. Right panel: Height (Z_{cm}), polar angle (θ), and number of rebounds $N_{rebounds}$. (a) E_i = 1.0 eV with T_s = 2000 K, (b) E_i = 2.0 eV with T_s = 520 K.

In the low energy regime, however, the study of the dissociative adsorption process requires the inclusion of indirect mechanisms, in which dynamic trapping plays a role. Let us analyze in detail the different dynamics involved in the two regimes. In order to get enough statistics, we will use different surface temperatures. According to Fig. 6, the results for instance, for E_i = 1.00 eV at T_s = 2000 K and for E_i = 2.00 eV at T_s = 520 K, give rise to roughly the same sticking probability. Hence, in Fig. 7, we show the positions of the dissociated molecules for these two incidence conditions, at the time at which the trajectory is identified as one leading to dissociation (*i.e.*, when r_{diss} = 2.1125 Å). For both kinetic energies, the positions of the center of mass (X_{cm},Y_{cm}) of the dissociated molecules over the unit cell show that the dissociation occurs close to the position of the third layer atoms. The molecules are dissociated at heights below 1.0 Å from the surface and with an orientation parallel to the surface. Although the final positions of the dissociated molecules are very similar, the histogram of the number of rebounds before they eventually dissociate is different for the two kinetic energies. For T_s = 520 K and E_i = 2.00 eV (Fig. 7b), the majority of molecules are dissociated after a small number of surface rebounds (*i.e.* direct mechanism). For T_s = 2000 K and E_i = 1.00 eV (Fig. 7a), however, the dissociation process is characterized by a high number of rebounds at the surface. We have verified that these rebounds are produced in the vicinity of the ε adsorption well. In the latter case, the majority of the molecules are first accommodated at the surface and exchange energy with the surface phonons before becoming dissociated. Previous work on the dissociation process of N_2 on Fe(111) suggested that, at low kinetic energy, the N_2 molecules are dissociated through an intermediate state.[24] Our dynamical calculations suggest that this is indeed the case.

Fig. 8 and 9 explain the details of the dynamics for the dissociative adsorption process, for normal incidence. Two different cases are considered: E_i = 1.00 and 2.00 eV at T_s = 2000 K. These cases, even if the temperature is unrealistic as mentioned before, are chosen to be representative of some indirect dynamics. The upper panel represents snapshots of the center of mass coordinates of the dissociated molecules, as well as that of the reflected ones, over the surface unit cell, upon reaching for the first time a distance *Z* from the surface. Additional information on top of each graph indicates the relative number of dissociated molecules that reach this distance *Z*, which will eventually be dissociated (N_Z^{stick}) and reflected ($N_Z^{reflect}$). The polar distribution of the dissociated molecules is shown in the lower panel.

Focusing on the eventually dissociated molecules, it is shown in Fig. 8 that all dissociated molecules reach the distance *Z* = 2.0 Å from the surface, keeping the positions of the center of mass (*X*,*Y*) and the molecular orientations (θ) very similar to the initial ones (not shown here). The same number of trajectories is recorded at *Z* = 1.0 Å, with a modified arrangement of molecular positions and orientations over the surface. Molecules are now placed close to the hollow site as well as close to the third layer atoms. Further movement toward the surface gives rise to molecular dissociation events below *Z* = 1.0 Å. We conclude that, for this energy range, the molecules are dissociated in the vicinity of the third layer atoms with their axis oriented parallel to the surface, with an azimuthal orientation such that one of the atoms is located near the atomic adsorption well at the hollow site and the other atom is oriented towards the next atomic adsorption site (see Fig. 5 in ref. 41). Fig. 9 shows that the dynamics and the final position for dissociation are similar for E_i = 2.0 eV, with some additional, though marginal, channel opened for dissociation close to the second layer atoms, and around the hollow site.

The experimentally[23–29] accepted general picture for the dissociation dynamics of N_2 on Fe(111) in the thermal regime assumes that the N_2 molecules are first attracted to the surface and accommodated perpendicularly on top of the first layer

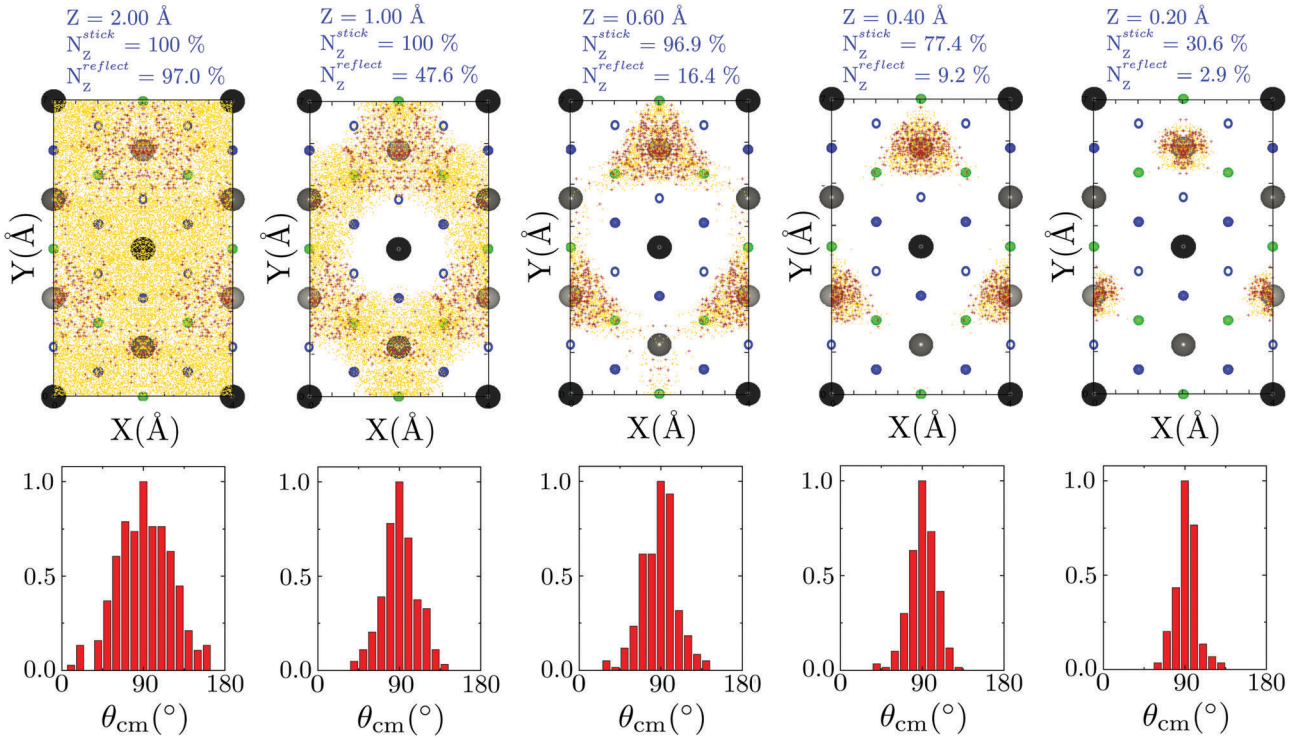

Fig. 8 Dynamical evolution of the N_2 molecules that eventually dissociate. The incidence is normal to the surface. The initial impact energy E_i = 1.0 eV. The surface temperature is T_s = 2000 K. 100 000 trajectories are included in the calculation. The upper panel shows the (X,Y) positions of the molecular center of mass upon reaching a given Z-distance from the surface for the first time. The red (yellow) symbols show the molecules that become eventually dissociated (reflected). Above each plot, the relative number of molecules reaching this Z-distance, among those finally dissociated (N_Z^{stick}) or reflected ($N_Z^{reflect}$), is shown. The lower panel shows the polar angle θ distribution for the dissociating molecules.

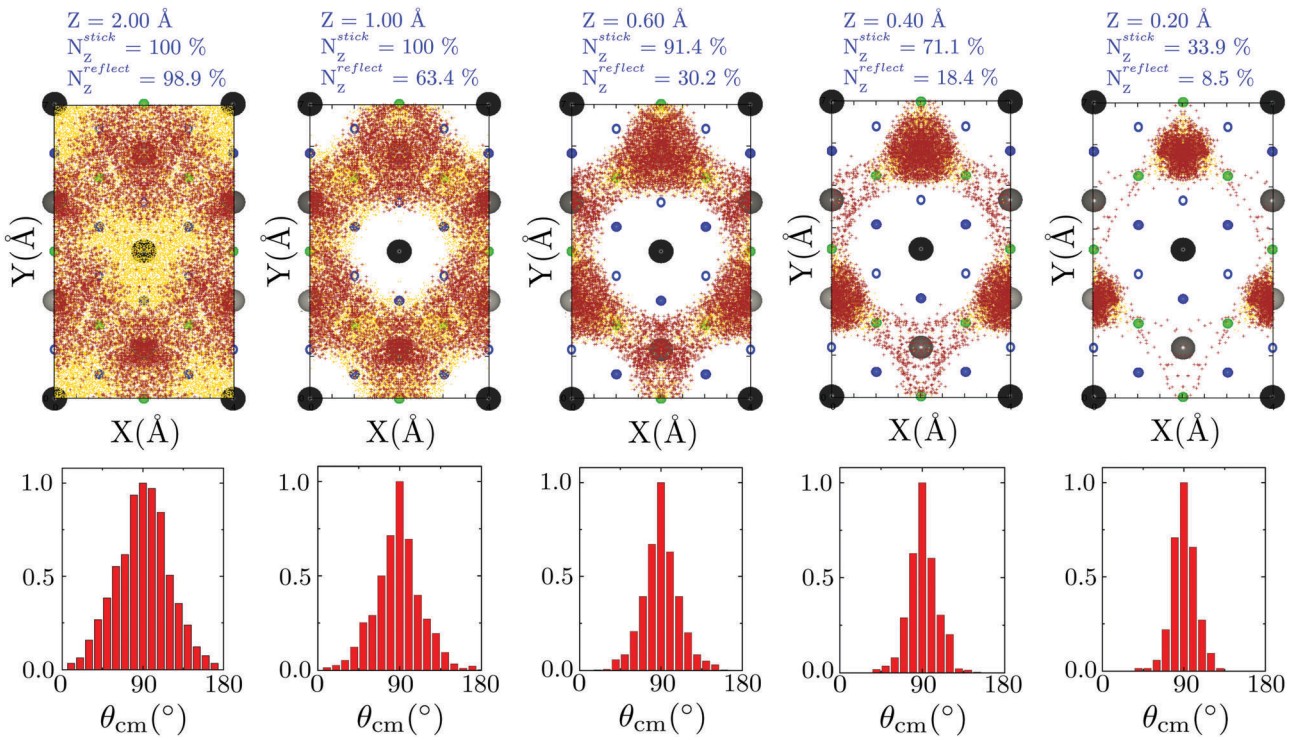

Fig. 9 Same as Fig. 8 with an initial incidence energy E_i = 2.0 eV and T_s = 2000 K.

atoms (γ-state), without any entrance barrier. From this position, the N_2 molecules start rotating their axis from the surface normal and move further toward the surface overcoming a potential barrier (from γ- to α-state). In the last step, the molecules dissociate from the molecularly adsorbed α-state into the atomically adsorbed β-state. Moreover, direct adsorption into the α-state is known to be important at higher impact energies.[29] In ref. 22 and 23, it was experimentally estimated that the dissociation probability from the α-state to the β-state is of the order of 10^{-3}, and the rest of the molecules desorb to the vacuum when the temperature is increased. In our work, we can follow the dissociative adsorption dynamics for N_2 on Fe(111). However, we cannot compare our findings with this scenario because the molecular energies for which we can obtain significant statistics are much higher than the thermal energy regime in which the experimental information was obtained.

Fe(111) *versus* Fe(110)

As mentioned in the introduction, the reactivity of N_2 on Fe surfaces highly depends on the crystal face, with Fe(111) being the most reactive one and Fe(110) the least reactive one. In this context we introduce a comparison between the nitrogen interactions on Fe(111) and Fe(110) from a theoretical perspective. Goikoetxea *et al.* studied both static and dynamic features of the N_2/Fe(110) system.[32] They found two favorable molecular adsorption states over the surface. The deepest adsorption well lies parallel to the surface at the bridge site at $Z \approx 1.4$ Å, and with an adsorption energy of 298 meV (α-state). The other adsorption state is for a molecule perpendicularly adsorbed on top of the first layer atom, at $Z \approx 2.4$ Å, and with an adsorption energy of 184 meV (γ-state). For the two adsorption states, they obtained a large entrance barrier from the gas-phase toward the surface. This is already a qualitative difference between the two surfaces, because molecular adsorption is not activated in the Fe(111) case.

Concerning reactive processes, molecular dynamics simulations for normal incidence show that the dissociation process on Fe(110) occurs mainly when the molecules are oriented parallel to the surface and close to the hollow site. The activation barrier for this process is ≈1.6 eV and at the transition state the molecule lies parallel to the surface, over a bridge site, with its axis pointing to the nearest atomic adsorption site (hollow site). On the other hand, there are four preferential (non-dissociative) adsorption states of N_2 at the Fe(111) surface (*i.e.* γ, δ, α, and ε). Besides the adsorption into the hollow site (α-state) there are adsorption states on the first, second and third layer atoms of the surface, characterized by large adsorption energy wells (450–640 meV). A necessary step in the dissociation process for both systems is that the molecule reaches a configuration parallel to the surface with an azimuthal orientation such that at least one N atom points toward the atomic adsorption site of the 3D atomic PES. Also, the dissociation dynamics is ruled in both cases by narrow paths leading to the dissociated state. In the case of Fe(111), however, we report dissociative events at 800 meV, an energy barrier which is half of the one for the Fe(110) surface.

In general, the difference in the reactivity between the two surfaces is due to the different activation barriers. The openness of the Fe(111) surface makes the second and third layer atoms exposed to the N_2 molecules, which results in more available molecular adsorption sites on the surface (α and ε states), and hence in a higher dissociation probability when compared to the close-packed Fe(110) surface. Experimentally, the higher reactivity of Fe(111) was attributed to the presence of C_7 coordination sites (number of nearest neighbours) of the N_2 for the second and third layer atoms,[4,21,22,60] which is in turn associated with a low surface work function and a high surface free energy. The experimental picture is consistent with our conclusion for the low entrance and dissociation barriers as well as with the calculated properties of nitrogen adsorption and dissociation dynamics in N_2/Fe(111).

4. Conclusion

We have presented a full dynamical study for the dissociative adsorption dynamics of N_2 on clean Fe(111) surfaces. First, we performed quasi-classical trajectory calculations on a DFT-based 6D-PES to obtain the initial dissociative sticking probability S_0. The quasi-classical calculations were performed for normal and off-normal incidence of N_2 molecules on the surface. The initial sticking probability shows high dependence on the incidence angle. A comparison with molecular beam experimental observations was introduced. Our results show sticking probabilities in general lower than the measured ones. A possible reason for this difference is that a large percentage of the incoming molecules remain dynamically trapped in an adsorption well. We have performed additional calculations for very high surface temperature in order to roughly estimate the ratio of the trapped molecules that will eventually dissociate. The theoretical results for molecular dissociation at high surface temperature show better agreement with the available experiments. Details of the dynamics indicate that most of the dissociated molecules approach the surface with the molecular axis roughly parallel to it. Dissociation occurs close to the third layer atoms, with a molecular azimuthal orientation such that one of the N atoms is very close to the hollow site and the other one points toward the next possible atomic adsorption state. We also introduced a comparison between our current work and previous work on Fe(110) for understanding the difference in reactivity for the two surfaces. Fe(111) shows a higher reactivity mainly due to the low entrance and activation barriers for N_2 compared with those of Fe(110), a conclusion which is consistent with the experimental studies.

Conflicts of interest

There are no conflicts to declare.

Acknowledgements

This work was partially supported by the Basque Departamento de Educación, Universidades e Investigación, the University of

the Basque Country UPV/EHU (Grant No. IT-756-13) and the Spanish Ministerio de Economía y Competitividad (Grants No. FIS2013-48286-C02-02-P and FIS2016-76471-P). M. A. N. acknowledges financial support by the Ministerio de Economía y Competitividad (Grant No. BES-2011-045536). Computational resources were provided by the DIPC Computing Center.

References

1 G. Ertl, *Encyclopedia of Catalysis*, John Wiley & Sons, Inc., 2002.
2 I. Rafiqul, C. Weber, B. Lehmann and A. Voss, *Energy*, 2005, **30**, 2487.
3 Y. Tanabe and Y. Nishibayashi, *Coord. Chem. Rev.*, 2013, **257**, 2551.
4 G. Ertl, *Catal. Rev.*, 1980, **21**, 201.
5 G. Ertl, *J. Vac. Sci. Technol., A*, 1983, **1**, 1247.
6 P. Stoltze and J. Nørskov, *J. Catal.*, 1988, **110**, 1.
7 F. Y. Hansen, N. E. Henriksen, G. D. Billing and A. Guldberg, *Surf. Sci.*, 1992, **264**, 225.
8 A. Hellman, *et al.*, *J. Phys. Chem. B*, 2006, **110**, 17719.
9 P. Iyngaran, D. C. Madden, S. J. Jenkins and D. A. King, *Proc. Natl. Acad. Sci. U. S. A.*, 2011, **108**, 925.
10 M. Kitano, S. Kanbara, Y. Inoue, N. Kuganathan, P. V. Sushko, T. Yokoyama, M. Hara and H. Hosono, *Nat. Commun.*, 2015, **6**, 6731.
11 G. A. Somorjai, *Introduction to surface chemistry and catalysis*, John Wiley & Sons, Inc., New York, 3rd edn, 1984.
12 R. Díez Muiño and H. F. Busnengo, *Dynamics of gas/surface interactions: Atomic-level understanding of scattering processes at surfaces*, Springer Series of Surface Sciences, Berlin, 2013.
13 B. Hammer and J. Nørskov, *Impact of Surface Science on Catalysis, Advances in Catalysis*, Academic Press, 2000, vol. 45, p. 71.
14 H. E. Pfnür, C. T. Rettner, J. Lee, R. J. Madix and D. J. Auerbach, *J. Chem. Phys.*, 1986, **85**, 7452.
15 C. T. Rettner, E. K. Schweizer, H. Stein and D. J. Auerbach, *Phys. Rev. Lett.*, 1988, **61**, 986.
16 C. T. Rettner, H. Stein and E. K. Schweizer, *J. Chem. Phys.*, 1988, **89**, 3337.
17 L. Martin-Gondre, C. Crespos, P. Larregaray, J. C. Rayez, B. van Ootegem and D. Conte, *J. Chem. Phys.*, 2010, **132**, 204501.
18 R. Pétuya, P.-A. Plötz, C. Crespos and P. Larregaray, *J. Phys. Chem. C*, 2014, **118**, 21904.
19 M. Alducin, R. Díez Muiño, H. F. Busnengo and A. Salin, *J. Chem. Phys.*, 2006, **125**, 144705.
20 M. Alducin, R. Díez Muiño, H. F. Busnengo and A. Salin, *Phys. Rev. Lett.*, 2006, **97**, 056102.
21 N. Spencer, R. Schoonmaker and G. Somorjai, *J. Catal.*, 1982, **74**, 129.
22 F. Bozso, G. Ertl, M. Grunze and M. Weiss, *J. Catal.*, 1977, **49**, 18.
23 G. Ertl, S. Lee and M. Weiss, *Surf. Sci.*, 1982, **114**, 515.
24 M. Grunze, M. Golze, W. Hirschwald, H. J. Freund, H. Pulm, U. Seip, M. C. Tsai, G. Ertl and J. Küppers, *Phys. Rev. Lett.*, 1984, **53**, 850.
25 M.-C. Tsai, U. Ship, I. Bassignana, J. Küppers and G. Ertl, *Surf. Sci.*, 1985, **155**, 387.
26 L. J. Whitman, C. E. Bartosch, W. Ho, G. Strasser and M. Grunze, *Phys. Rev. Lett.*, 1986, **56**, 1984.
27 L. J. Whitman, C. E. Bartosch and W. Ho, *J. Chem. Phys.*, 1986, **85**, 3688.
28 H.-J. Freund, B. Bartos, R. Messmer, H. Grunze, H. Kuhlenbeck and M. Neumann, *Surf. Sci.*, 1987, **185**, 187.
29 M. Grunze, G. Strasser and M. Golze, *Appl. Phys. A: Solids Surf.*, 1987, **44**, 19.
30 J. Mortensen, M. Ganduglia-Pirovano, L. Hansen, B. Hammer, P. Stoltze and J. Nørskov, *Surf. Sci.*, 1999, **422**, 8.
31 S. Riikonen, A. S. Foster, A. V. Krasheninnikov and R. M. Nieminen, *Phys. Rev. B: Condens. Matter Mater. Phys.*, 2009, **80**, 155429.
32 I. Goikoetxea, M. Alducin, R. Díez Muiño and J. I. Juaristi, *Phys. Chem. Chem. Phys.*, 2012, **14**, 7471.
33 S. Pick, P. Légaré and C. Demangeat, *Phys. Rev. B: Condens. Matter Mater. Phys.*, 2007, **75**, 195446.
34 I. Goikoetxea, J. I. Juaristi, R. Díez Muiño and M. Alducin, *Phys. Rev. Lett.*, 2014, **113**, 066103.
35 I. Goikoetxea, M. Alducin, R. Díez Muiño and J. I. Juaristi, *Phys. Chem. Chem. Phys.*, 2015, **17**, 19432.
36 D. Tománek and K. H. Bennemann, *Phys. Rev. B: Condens. Matter Mater. Phys.*, 1985, **31**, 2488.
37 J. Mortensen, L. Hansen, B. Hammer and J. Nørskov, *J. Catal.*, 1999, **182**, 479.
38 T. Panczyk, *J. Phys. Chem. C*, 2007, **111**, 3175.
39 T. Wang, X. Tian, Y. Yang, Y.-W. Li, J. Wang, M. Beller and H. Jiao, *J. Phys. Chem. C*, 2016, **120**, 2846.
40 M. A. Nosir, L. Martin-Gondre, G. A. Bocan and R. Díez Muiño, *Nucl. Instrum. Methods Phys. Res., Sect. B*, 2016, **382**, 105.
41 M. A. Nosir, L. Martin-Gondre, G. A. Bocan and R. Díez Muiño, *Phys. Chem. Chem. Phys.*, 2017, **19**, 7370.
42 C. T. Rettner and H. Stein, *Phys. Rev. Lett.*, 1987, **59**, 2768.
43 P. Hohenberg and W. Kohn, *Phys. Rev.*, 1964, **136**, B864.
44 W. Kohn and L. J. Sham, *Phys. Rev.*, 1965, **140**, A1133.
45 G. Kresse and J. Furthmüller, *Phys. Rev. B: Condens. Matter Mater. Phys.*, 1996, **54**, 11169.
46 G. Kresse and D. Joubert, *Phys. Rev. B: Condens. Matter Mater. Phys.*, 1999, **59**, 1758.
47 P. E. Blöchl, *Phys. Rev. B: Condens. Matter Mater. Phys.*, 1994, **50**, 17953.
48 J. P. Perdew, J. A. Chevary, S. H. Vosko, K. A. Jackson, M. R. Pederson, D. J. Singh and C. Fiolhais, *Phys. Rev. B: Condens. Matter Mater. Phys.*, 1992, **46**, 6671.
49 J. P. Perdew and Y. Wang, *Phys. Rev. B: Condens. Matter Mater. Phys.*, 1992, **45**, 13244.
50 H. J. Monkhorst and J. D. Pack, *Phys. Rev. B: Condens. Matter Mater. Phys.*, 1976, **13**, 5188.
51 S. R. Hall and B. McMahon, *International Tables for Crystallography Volume G: Definition and Exchange of Crystallographic*

Data, International Tables for Crystallography G, Springer, Netherlands, 2005.
52 C. Kittel, *Introduction to Solid State Physics*, John Wiley & Sons, Inc., New York, 6th edn, 1986.
53 H. F. Busnengo, A. Salin and W. Dong, *J. Chem. Phys.*, 2000, **112**, 7641.
54 R. A. Olsen, H. F. Busnengo, A. Salin, M. F. Somers, G. J. Kroes and E. J. Baerends, *J. Chem. Phys.*, 2002, **116**, 3841.
55 C. Díaz, R. A. Olsen, H. F. Busnengo and G. J. Kroes, *J. Phys. Chem. C*, 2010, **114**, 11192.
56 S. A. Adelman and J. D. Doll, *J. Chem. Phys.*, 1976, **64**, 2375.
57 J. C. Tully, *J. Chem. Phys.*, 1980, **73**, 1975.
58 H. F. Busnengo, M. A. Di Césare, W. Dong and A. Salin, *Phys. Rev. B: Condens. Matter Mater. Phys.*, 2005, **72**, 125411.
59 F. Bozso, G. Ertl and M. Weiss, *J. Catal.*, 1977, **50**, 519.
60 D. Strongin, J. Carrazza, S. R. Bare and G. Somorjai, *J. Catal.*, 1987, **103**, 213.